J Mater Sci: Mater Electron
DOI 10.1007/s10854-015-4085-x

Different-layered $Ni(OH)_2$ nanoflakes/3D graphene composites for flexible supercapacitor electrodes

Wei Lan[1,2] · Guomei Tang[2] · Yaru Sun[2] · Yupeng Wei[1] · Peiqing La[1] · Qing Su[2] · Erqing Xie[2]

Received: 20 August 2015 / Accepted: 15 November 2015

Abstract Monolayer and multilayer $Ni(OH)_2$ nanoflakes/3D graphene composites were successfully prepared by modulating the seed layer of $Ni(OH)_2$ in a hydrothermal synthesis. An important advantage is that no other inactive binder is required to be utilized in the composite electrode to produce a flexible supercapacitor. It is found that the 3D graphene grown via CVD has a limited contribution to the overall capacitance when solely utilized as a current collector, while $Ni(OH)_2$ nanoflakes have been determined to be the primary contributor to the overall capacitance of the device. The electrochemical properties of monolayer $Ni(OH)_2$ nanoflakes/3D graphene are significantly enhanced relative to multilayer $Ni(OH)_2$ nanoflakes/3D graphene. At 10 A/g current density, a high specific capacitance of 1606 F/g (per total mass of electrodes) is obtained for monolayer $Ni(OH)_2$ nanoflakes/3D graphene composites. After 1000 cycles of charge/discharge, cycling performance shows 96 % capacitance retention at 10 A/g current density.

✉ Wei Lan
lanw@lzu.edu.cn

[1] State Key Laboratory of Advanced Processing and Recycling of Non-ferrous Metals, Lanzhou University of Technology, Lanzhou 730050, People's Republic of China

[2] Key Laboratory for Magnetism and Magnetic Materials of Ministry of Education, School of Physical Science and Technology, Lanzhou University, Lanzhou 730000, People's Republic of China

1 Introduction

Supercapacitor, or electrochemical capacitor, has been widely studied because of its unique combination of high power density and long cycle life relative to batteries and capacitors [1]. Pseudocapacitors are a classification of supercapacitors that are capable of storing energy from rapid reversible Faradaic redox reactions on the surface and the near surface of the electrode, which has been a promising focus in the field of energy storage [2]. Literature shows that the electrochemical performance of pseudocapacitors is mainly due to the high specific surface area and the high reversible electrochemical reaction of the electrode materials [3]. At present, the electrode material of pseudocapacitors is primarily concentrated in the utilization of transition metal oxides, hydroxides and conductive polymers [2–8]. However, pseudocapacitors depend on the rate of electron transport, ion diffusion, and the reaction reversibility, which is due to the limit of the redox kinetics [9]. The higher specific surface area and electrical conductivity can improve the capacitance performance of electrode materials.

Nickel hydroxide ($Ni(OH)_2$) is commonly used as a battery electrode due to its superior physical, chemical and electrochemical properties. However, due to its poor conductivity, $Ni(OH)_2$ has to require a synergistic effect combined with other conductive materials, as well as a high specific surface area to enhance its properties of electron transport and ion diffusion [10–12]. As a typical 2D material, graphene has unique electronic properties, as well as excellent mechanical, optical, thermal and electrochemical properties that make it the ideal material for capacitor electrodes [13, 14]. Moreover, graphene can be utilized as a unique 2D structure unit to assemble a 3D macroscopic material with controllable microstructure that

Published online: 09 December 2015

can be directly applied in the manufacturing of self-supported supercapacitor electrodes without any conductive additive or binder. It was found that the diffusion time of electrolyte ions (t) is proportional to the square of the diffusion length (L) ($t \approx L^2/D$) in the electrode of supercapacitors [15, 16]. Therefore, it is very important to prepare nanoscale $Ni(OH)_2$ active materials with a short diffusion distance and abundant exposure to active sites. It should also form a synergistic complex with 3D graphene in order to improve the electrochemical performance of $Ni(OH)_2$-based supercapacitor electrodes.

In this paper, 3D graphene was grown by CVD method and $Ni(OH)_2$ nanoflakes with a different number of layers were directly synthesized on the surface of 3D graphene by modulating seed layer via hydrothermal process. A flexible supercapacitor electrode was constructed by combining 3D graphene and $Ni(OH)_2$ nanoflakes sans binder between them. The electrochemical performance and mechanism of capacitance were studied in detail.

2 Experimental section

2.1 Preparation of 3D graphene

3D graphene was grown on a foam nickel substrate by using ethanol as the carbon source [17–19]. The Ni foams (380 g/m^2 and 1.5 mm thick, pressed to 0.5 mm) were thoroughly cleaned and placed in a tube furnace. Before heating, 200 sccm Ar was introduced and maintained for 15 min to remove the air in the system. Then, the airflow of 100 sccm Ar and 50 sccm H_2 was kept constant, the furnace temperature increased to 1000 °C and maintained for 30 min. Ethanol was loaded into the chamber for 20 min. The furnace temperature quickly dropped to room temperature with a cooling rate of ~100 °C/min. The Ni substrate was etched by 3 HCl mol/L at 80 °C and then carefully cleaned to remove residual impurities. Lastly, the self-supported 3D graphene was obtained after drying.

2.2 Synthesis of $Ni(OH)_2$ nanoflakes

The chemical reagents were analytical grade and used without further purification. Nickel nitrate ($Ni(NO_3)_2 \cdot 6H_2O$) and hexamethylenetetramine (HMT, $C_6H_{12}N_4$) were purchased from Sigma Aldrich Co. LLC. The deionized water was utilized as the solvent and the volume of reaction solution was fixed at 35 mL.

The mixed solution of 0.402 g $Ni(NO_3)_2 \cdot 6H_2O$ and 1.008 g HMT was used to grow the seed layer. 3D graphene was immersed in ethanol solution for 10 s, the mixed solution for 10 s and then taken out to dry. The process was repeated five times to produce the seed layer. 0.201 g $Ni(NO_3)_2 \cdot 6H_2O$ and 0.504 g HMT were dissolved in deionized water and then transferred to an autoclave with 50 mL volume. After the 3D graphene was submerged in the reaction solution, the autoclave was kept at 80 °C for 8 h. The deionized water and ethanol were used to repeatedly rinse and sonicate the samples. The multilayer $Ni(OH)_2$ nanoflakes/3D graphene composites with the seed layer was produced after drying at 65 °C for 3 h. By removing the procedure of seed layer growth, the single layer $Ni(OH)_2$ nanoflakes/3D graphene composites are obtained rather than a multilayer form.

2.3 Characterization

The morphologies of the samples were observed by field emission scanning electron microscopy (FE-SEM, Hitachi S-4800). The microstructures were characterized using transmission electron microscopy (TEM, FEI Tecnai F30, operated at 300 kV) equipped with an X-ray energy dispersive spectrometer (EDS). The crystal structures of the samples were examined by X-ray diffraction (XRD, Philips, X'pert pro, Cu Kα, 0.154056 nm) and Raman spectroscopy (JY-HR800 micro-Raman, using a 532 nm wavelength YAG laser with a laser spot diameter of ~600 nm). The mass of $Ni(OH)_2$ active materials was measured by a microbalance (Mettler, XS105DU) with an accuracy of 0.01 mg. Electrochemical measurements (CHI 660E Electrochemical Workstation) were carried out in a three-electrode electrochemical cell in a 1 M NaOH aqueous electrolyte. The samples were used directly as the working electrodes. A Pt plate and an Hg/HgO electrode were used as the counter electrode and the reference electrode, respectively. All the potentials were referred to the reference electrode.

3 Results and discussion

$Ni(NO_3)_2 \cdot 6H_2O$ and $C_6H_{12}N_4$ are utilized as raw materials, the main chemical reactions occurring in the hydrothermal conditions are as follows:

$$Ni^{2+} + xNR_3 + (6-x)H_2O \leftrightarrow \left[Ni(NR_3)_x \cdot (H_2O)_{6-x}\right]^{2+} \quad (1)$$

$$\left[Ni(NR_3)_x \cdot (H_2O)_{6-x}\right]^{2+} \xleftrightarrow{\Delta} Ni(OH)(H_2O)_{5-x}(NR_3)_{x-1} + HNR_3^+ \quad (2)$$

$$Ni(OH)(H_2O)_{5-x}(NR_3)_{x-1} \leftrightarrow Ni(OH_2)(OH_2)_{4-x}(NR_3)_{x-2} + HNR_3^+ \quad (3)$$

$$\mathrm{Ni(OH_2)(OH_2)_{4-x}(NR_3)_{x-2}} \leftrightarrow \mathrm{Ni(OH)_2} \downarrow + (4-\mathrm{x})\mathrm{H_2O} + (\mathrm{x}-2)\mathrm{NR_3} \quad (4)$$

After completing the above-depicted reaction, $Ni(OH)_2$ nanoflakes are grown and attached on the surface of 3D graphene.

Figure 1a is the XRD patterns of $Ni(OH)_2$ nanoflakes/3D graphene composites combined via CVD and hydrothermal processes. As seen, in addition to the two diffraction peaks from the 3D graphene, newly formed diffraction peaks are corresponding to the (001), (100) and (101) crystal plane of $Ni(OH)_2$ (JCPDS No.14-0117). The Raman spectra in Fig. 1b also demonstrates that the composite materials have a Raman shift peak at $\sim 510\ cm^{-1}$ that is related to $Ni(OH)_2$ nanoflakes. Both characterization techniques indicate that $Ni(OH)_2$ and graphene composites have been successfully prepared.

Figure 2 shows the SEM images of 3D graphene after etching away Ni foam substrate. As seen from Fig. 2a, the self-supported 3D graphene inherits its structure from the architecture of the Ni foam substrate, which enables the graphene to possess a larger specific surface area. It can be clearly seen that there are a large number of wrinkles on the surface of 3D graphene (Fig. 2b). The wrinkles are generated from the rapid cooling step during the CVD growth process, which originates from the different thermal expansion and shrinkage coefficients between Ni foam and graphene. The wrinkles promote the nucleation of $Ni(OH)_2$ nanoflakes on the surface of 3D graphene. Figure 3 shows SEM images of $Ni(OH)_2$ nanoflakes/3D graphene composites with and without a seed layer in the hydrothermal process step. The grown samples without a seed layer (Fig. 3a) exhibit an evenly distributed single layer of $Ni(OH)_2$ nanoflakes on the 3D graphene. However, after planting the seed layer, the multilayer $Ni(OH)_2$ nanoflakes (Fig. 3b) are obtained by stacked nanoflakes in the vertical direction, originating from the fact that the seed layer is beneficial to the rapid growth of $Ni(OH)_2$ nanoflakes on the 3D graphene.

Figure 4 displays TEM images of 3D graphene and $Ni(OH)_2$ nanoflakes/3D graphene composites. It can be seen that 3D graphene composed of a few layers is very lightly colored and transparent. As seen from Fig. 4b, the nanoflakes display a translucent sheet structure. Under high resolution observation, the crystal plane spacing of 0.234 nm illustrates that they correspond to the (101) crystal surface of $Ni(OH)_2$, which further proves the lamellar structure of $Ni(OH)_2$. Therefore, the images demonstrate the successful synthesis of $Ni(OH)_2$ nanoflakes/3D graphene composites.

$Ni(OH)_2$ nanoflakes/3D graphene composites have a potential for application as the electrodes in supercapacitor devices; therefore, the electrochemical performance of the composite was characterized. The prepared $Ni(OH)_2$ nanoflakes/3D graphene composites are utilized as the working electrode. The area of working electrode involved in the electrochemical reaction is $1 \times 1\ cm^2$. Figure 5a shows the galvanostatic charge/discharge characteristics of the 3D graphene and $Ni(OH)_2$ nanoflakes/3D graphene composites. The voltage range is 0–0.6 V and the charge/discharge current density is 10 A/g. As seen, under the same current density, the charge/discharge time of $Ni(OH)_2$ nanoflakes/3D graphene composites is significantly longer than that of 3D graphene. The relatively short period of charge and discharge indicates that the specific capacity of 3D graphene grown by CVD can be neglected and be considered to behave as a current collector while the $Ni(OH)_2$ nanoflakes are the component that primarily contributes to the specific capacitance of the supercapacitor electrode. From the cyclic voltammetry properties of 3D graphene and $Ni(OH)_2$ nanoflakes/3D graphene composites (Fig. 5b), it can also be demonstrated that the 3D graphene essentially lacks any electrochemical behavior.

Figure 6a portrays the galvanostatic charge/discharge curves of the monolayer and multilayer $Ni(OH)_2$

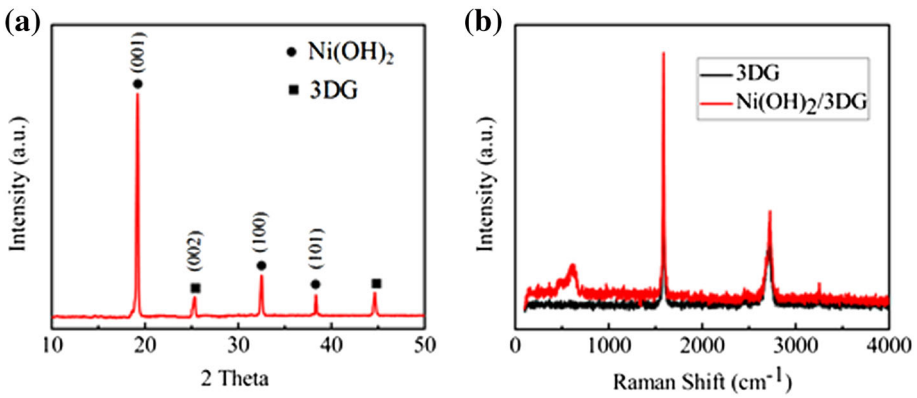

Fig. 1 **a** XRD patterns of $Ni(OH)_2$ nanoflakes/3D graphene composite and pristine 3D graphene. **b** Raman spectra of 3D graphene and $Ni(OH)_2$

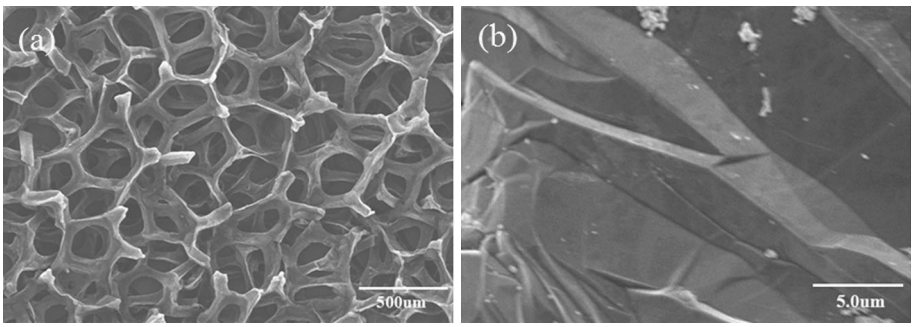

Fig. 2 SEM images of 3D graphene after etching away Ni foams, **a** low magnification, **b** high magnification

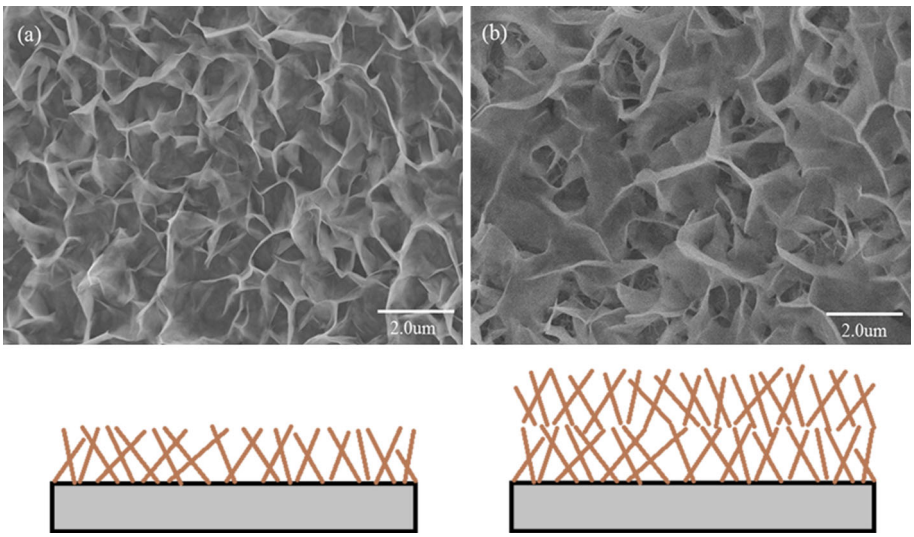

Fig. 3 SEM images and section schematic diagrams of monolayer (**a**) and multilayer (**b**) $Ni(OH)_2$ nanoflakes/3D graphene composites

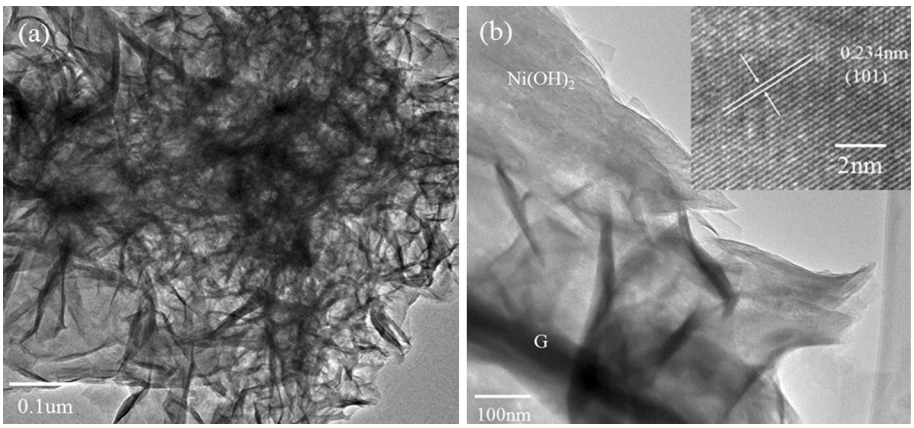

Fig. 4 TEM images of **a** 3D graphene and **b** $Ni(OH)_2$ nanoflakes/3D graphene composites

nanoflakes/3D graphene composites. Under the same charge/discharge current density (10 A/g), the charge/discharge time of the single layer $Ni(OH)_2$ nanoflakes/3D graphene composites is significantly larger than that of the multilayer composite, which is verified from by the cyclic voltammetric properties of the samples. Under the same scan rate (15 mV/s), the hysteresis curve area of the monolayer $Ni(OH)_2$ nanoflakes/3D graphene composites is substantially greater than the multilayer composite. The specific capacitance value, Cs, can be calculated by the following formula:

$$Cs = It/(m\Delta V) \tag{5}$$

Here I is the charge and discharge current, t is the discharge time, ΔV is the range of the voltage from a charged to a discharged state, and m is the quality of active material,

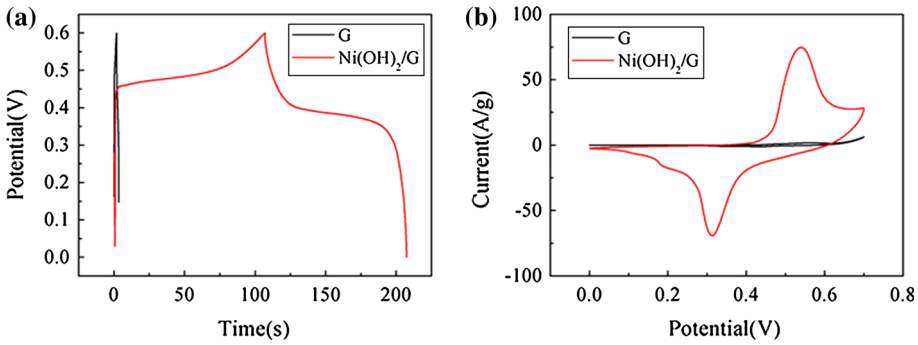

Fig. 5 Electrochemical properties of 3D graphene and $Ni(OH)_2$ nanoflakes/3D graphene composites, **a** the galvanostatic charge/discharge characteristics, **b** the cyclic voltammetry properties

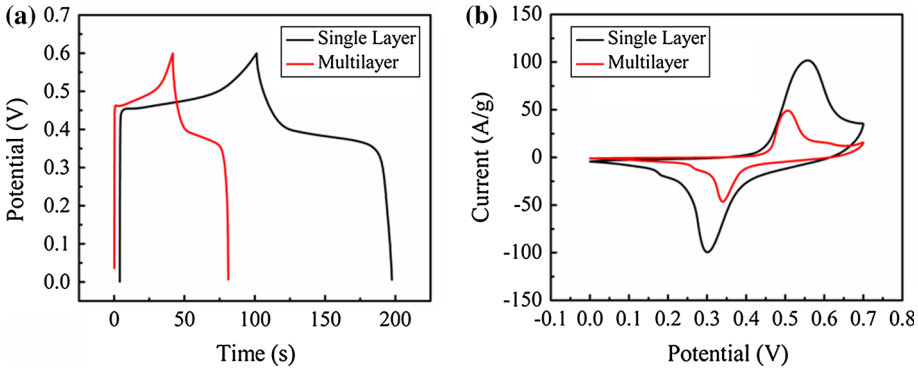

Fig. 6 Electrochemical properties of the monolayer and multilayer $Ni(OH)_2$ nanoflakes/3D graphene composites, **a** the galvanostatic charge/discharge characteristics, **b** the cyclic voltammetry properties

which can be obtained by difference of the sample weighed before and after $Ni(OH)_2$ hydrothermal synthesis. The specific capacitance values for the monolayer and multilayer $Ni(OH)_2$ nanoflakes/3D graphene composites are 1606 and 833 F/g, respectively. These results suggest that the monolayer $Ni(OH)_2$ nanoflakes/3D graphene composites have enhanced electrochemical properties, more specifically the specific capacitance. The observed properties might be attributed to the direct contact between $Ni(OH)_2$ nanoflakes and 3D graphene, which leads to a shortened path of electron transport and ion diffusion in the monolayer $Ni(OH)_2$ nanoflakes/3D graphene composites. Even though the multilayer composites possess more active material, the specific capacitance that is usually proportional to the active area could not be effectively enhanced. Therefore, The active material content of $Ni(OH)_2$ nanoflakes is very important in the modulation of the electrochemical performance of supercapacitor electrodes.

In order to further characterize the electrochemical properties of the single layer $Ni(OH)_2$ nanoflakes/3D graphene composites, the following tests were carried out. Figure 7a shows the cyclic voltammetric curves of the monolayer $Ni(OH)_2$ nanoflakes/3D graphene composites at the scan rates of 5, 10, 20, 30, 40, 15 and 50 mV/s. It can be seen that a pair of obvious redox peaks are observed that indicate a reversible redox reaction in the charge/discharge process [20]. The oxidation peak is due to the oxidation process from α-$Ni(OH)_2$ to γ-NiOOH. On the contrary, the reduction process from γ-NiOOH to α-$Ni(OH)_2$ produces the reduction peak. The electrochemical reaction is as follows:

$$\alpha - Ni(OH)_2 + OH^- \leftrightarrow \gamma - NiOOH + H_2O + e^- \quad (6)$$

The shape of the cyclic voltammetric curves is well maintained when the scan rate increases from 5 to 50 mV/s, demonstrating that the composites have an excellent electrochemical reversibility and rate capability. With the increase of scan rate, the oxidation and reduction peaks are slightly shifted to the forward and reverse direction, respectively. This might be due to the tortuous diffusion path of OH^- ions in $Ni(OH)_2$ active material as well as the native resistance of the supercapacitor electrode. At high scan rates, the relaxation time of a redox reaction becomes limited, suppressing the effective diffusion of OH^- ions that making the surface depth of the charge-storing $Ni(OH)_2$ nanoflakes relatively shallow. However, at low scan rates, more of the surface active material is adequately being utilized to store charge and the diffusion of OH^- ions has a large depth that allows for a high specific capacitance value to be obtained.

In comparison to the cyclic voltammetry curve, a more accurate specific capacitance could be calculated from the galvanostatic current charge/discharge curve [21]. The galvanostatic charge/discharge test is performed at different current densities. Figure 7b shows the galvanostatic charge/discharge curves measured at 10, 20, 30, 40, 60 and

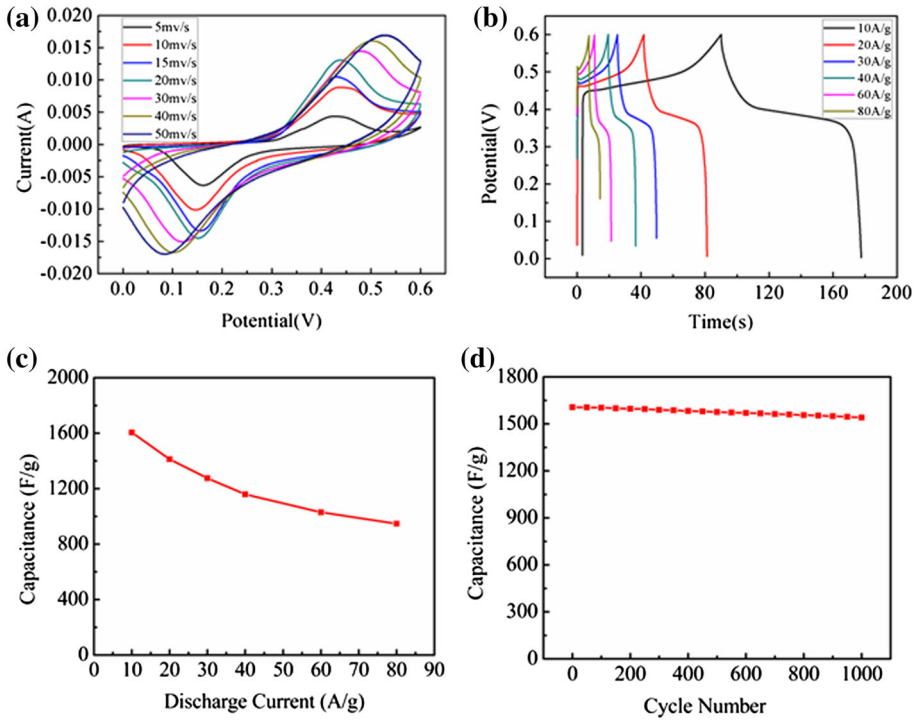

Fig. 7 **a** CV curves of the monolayer $Ni(OH)_2$ nanoflakes/3D graphene composites as the electrode material at various scan rates; **b** Galvanostatic charge/discharge *curves* at various current densities; **c** The calculated capacitance as a function of current density; **d** Cycling performance of the monolayer $Ni(OH)_2$ nanoflakes/3D graphene composites over 1000 cycles at a current density of 10 A/g

80 A/g. According to the results in Fig. 7b, the specific capacitance of monolayer $Ni(OH)_2$ nanoflakes/3D graphene composites at different current densities is calculated (Fig. 7c). It can be found that the specific capacitance value gradually reduces as current density increases. For 10 A/g current density, the calculated specific capacitance value is 1606 F/g. When the current density is increased to 80 A/g, the specific capacitance is 947 F/g, which demonstrates a capacitance retention of ~60 % when the current density increases by a factor of 8. The capacitance value is obviously higher than previously reported results. Wen et al. [22] calculated a specific capacitance of 950 F/g according to the discharge curves of $Ni(OH)_2$ nanosheet electrode at a current density of 0.5 A/g. Liu et al. [23] obtained the specific capacitance of 631 F/g at a discharge current density of 10 A/g for pure $Ni(OH)_2$ nanoparticles and improves to 905 F/g after combining with reduced graphene oxide. Bag et al. [24] obtained a specific capacitance of 1339.13 F/g for layered hybrid rGO/α-$Ni(OH)_2$ electrodes at a current density of 10 A/g. Ma et al. [25] prepared a 3D flower-like β-$Ni(OH)_2$/GO/CNTs composite and found that the specific capacitance based on the mass of $Ni(OH)_2$ was ~1060 F/g at 10 A/g. This electrochemical performance indicates that the $Ni(OH)_2$/3D graphene composites are capable of achieving the requirements of different discharge power demands for practical applications.

In addition to the high specific capacitance, the cyclic stability is also a very important parameter to evaluate the electrochemical properties of supercapacitor electrodes. Under the current density of 10 A/g, the cycle test of charge/discharge has been carried out. Figure 7d shows the average specific capacitance calculated after 50 cycles. After running 1000 cycles, the specific capacitance remains 96 % of its initial value, which directly proves the $Ni(OH)_2$ nanoflakes/3D graphene composite electrode has excellent cycle stability as applied in a supercapacitor.

In order to better understand the mechanism of excellent electrochemical performance for the monolayer $Ni(OH)_2$ nanoflakes/3D graphene composites, SEM images (Fig. 8) are collected after the 1000 charge/discharge cycles. It can

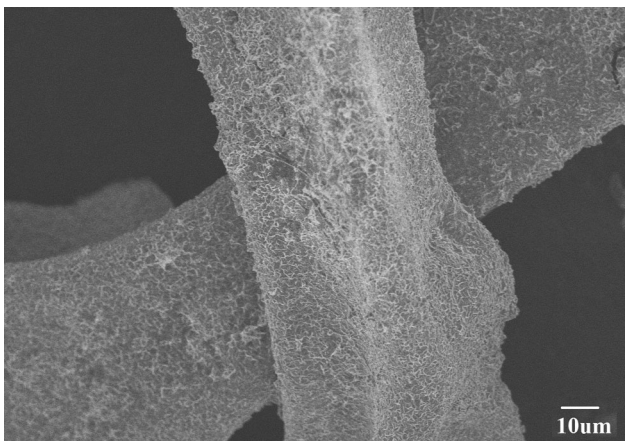

Fig. 8 SEM image of monolayer $Ni(OH)_2$ nanoflakes/3D graphene composites after the 1000 cycles

be seen that the intact structure of the $Ni(OH)_2$ nanoflakes are maintained without any obvious deformation, desquamation or collapsing. This phenomenon suggests that the synthesis strategy of CVD and hydrothermal growth has obvious advantages in the fabrication of $Ni(OH)_2$ nanoflakes/3D graphene composite electrodes.

4 Conclusions

$Ni(OH)_2$ nanoflakes/3D graphene composites of different layers were successfully synthesized to be utilized as a flexible supercapacitor electrode. Results demonstrate that 3D graphene grown via CVD acts as a pure current collector in terms of its minimal capacitance and resistance while $Ni(OH)_2$ nanoflakes behave as the active capacitive material. The number of layers of $Ni(OH)_2$ nanoflakes is very critical in terms of the electrochemical performance. An ideal hybrid supercapacitor electrode designed for electron transport and ion diffusion can be built by single layer $Ni(OH)_2$ nanoflakes on 3D graphene. The electrode composed with the multilayer $Ni(OH)_2$ nanoflakes and 3D graphene does not contribute to the expected proportionate capacitance behavior, which reduces the overall performance of the supercapacitor device. The result is of high significance for a promising material to fabricate the enhanced supercapacitor electrodes.

Acknowledgments This work was supported by Natural Science Foundation of Gansu Province (No. 1208RJZA199), the fund of the State Key Laboratory of Advanced Processing and Recycling of Nonferrous Metals, Lanzhou University of Technology (SKLAB02 014003), the Fundamental Research Funds for the Central Universities (No. lzujbky-2015-116) and the Project-sponsored by SRF for ROCS, SEM.

References

1. P. Simon, Y. Gogotsi, Nat. Mater. **7**, 845–854 (2008)
2. C.D. Wang, J.L. Xu, M.F. Yuen, J. Zhang, Y.Y. Li, X.F. Chen, W.J. Zhang, Adv. Funct. Mater. **24**, 6372–6380 (2014)
3. C.C. Hu, K.H. Chang, M.C. Lin, Y.T. Wu, Nano Lett. **12**, 2690–2695 (2006)
4. D.C. Iwueke, C.I. Amaechi, A.C. Nwanya, A.B.C. Ekwealor, P.U. Asogwa, R.U. Osuji, M. Maaza, F.I. Ezema, J. Mater. Sci.: Mater. Electron. **26**, 2236–2242 (2015)
5. T. Brezesinski, J. Wang, S.H. Tolbert, B. Dunn, Nat. Mater. **9**, 146–151 (2010)
6. X.X. Xiao, S. Li, H. Wei, D. Sun, Y.Z. Wu, G.Z. Jin, F. Wang, Y.P. Zou, J. Mater. Sci.: Mater. Electron. **26**, 4226–4233 (2015)
7. S. Nejati, T.E. Minford, Y.Y. Smolin, K.K.S. Lau, ACS Nano **8**, 5413–5422 (2014)
8. Y.M. He, W.J. Chen, X.D. Li, Z.X. Zhang, J.C. Fu, C.H. Zhao, E.Q. Xie, ACS Nano **7**, 174–182 (2013)
9. J. Liu, C. Cheng, W. Zhou, H. Li, H.J. Fan, Chem. Commun. **47**, 3436–3438 (2011)
10. J. Yan, Z.J. Fan, W. Sun, G.Q. Ning, T. Wei, Q. Zhang, R.F. Zhang, L.J. Zhi, F. Wei, Adv. Funct. Mater. **22**, 2632–2641 (2012)
11. M. Li, S.H. Xu, Y.P. Zhu, P.X. Yang, L.W. Wang, P.K. Chu, J. Alloys Compd. **589**, 364–371 (2014)
12. T. Xiao, B. Heng, X. Chen, J. Alloys Compd. **549**, 147–151 (2013)
13. Y.Z. Zhang, T. Liu, B. Meng, X.H. Li, G.Z. Liang, X.N. Hu, Q.J. Wang, Nat. Commun. **4**, 1811 (2013)
14. J. Xia, F. Chen, J. Li, N. Tao, Nat. Nanotech. **4**, 505–509 (2009)
15. S.B. Yang, Y.J. Gong, Z. Liu, L. Zhan, D.P. Hashim, L.L. Ma, R. Vajtai, P.M. Ajayan, Nano Lett. **13**, 1596–1601 (2013)
16. Y.G. Guo, J.S. Hu, L.J. Wan, Adv. Mater. **20**, 2878–2887 (2008)
17. W. Deng, Y.R. Sun, Q. Su, E.Q. Xie, W. Lan, Mater. Lett. **137**, 124–127 (2014)
18. W. Deng, W. Lan, Y.R. Sun, Q. Su, E.Q. Xie, Appl. Surf. Sci. **305**, 433–438 (2014)
19. W. Lan, Y.R. Sun, Y.X. Chen, J.Y. Wang, G.M. Tang, W. Dou, Q. Su, E.Q. Xie, RSC Adv. **5**, 20878–20883 (2015)
20. L.D. Feng, Y.F. Zhu, H.Y. Ding, C.Y. Ni, J. Power Sources **267**, 430–444 (2014)
21. M.D. Stoller, R.S. Ruoff, Energ. Environ. Sci. **3**, 1294–1301 (2010)
22. J. Wen, S.Z. Li, B.R. Li, Z.C. Song, H.N. Wang, R. Xiong, G.J. Fang, J. Power Sources **284**, 279–286 (2015)
23. Y.H. Liu, R.T. Wang, X.B. Yan, Sci. Rep. **5**, 11095 (2015)
24. S. Bag, C.R. Raj, J. Mater. Chem. A **2**, 17848–17856 (2014)
25. X.W. Ma, J.W. Liu, C.Y. Liang, X.W. Gong, R.C. Che, J. Mater. Chem. A **2**, 12692–12696 (2014)